Supporting Information

Predicting Ligand Removal Energetics in Thiolate-protected Nanoclusters from Molecular Complexes

Julia McKay[1], Michael J. Cowan[1], Cristian A. Morales-Rivera[1], and Giannis Mpourmpakis[1,*]

[1]Department of Chemical and Petroleum Engineering, University of Pittsburgh, Pittsburgh, PA 15261, USA

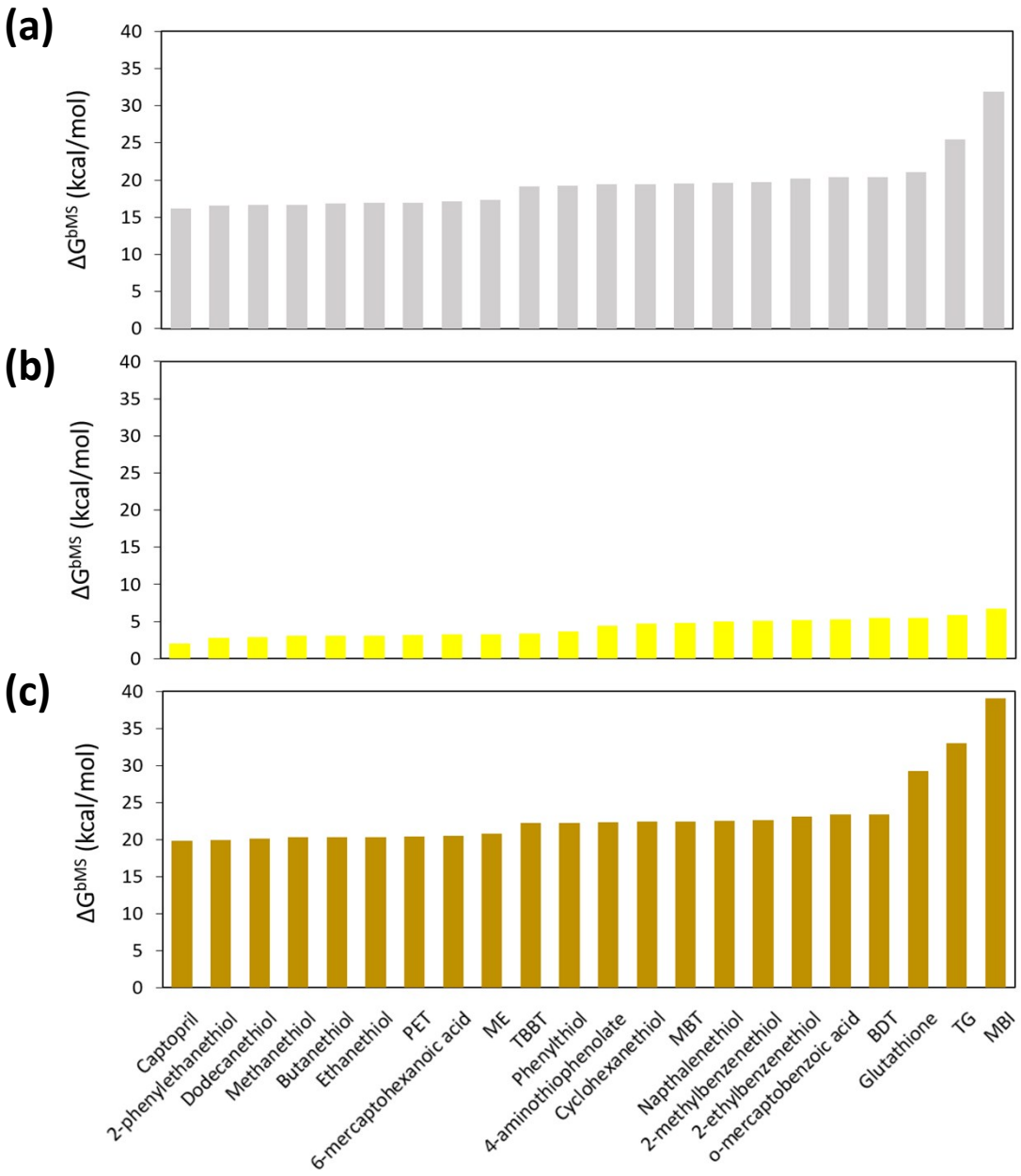

Figure S1. Bar graphs of Gibbs Free Energy of break M-S reaction for **(a)** Ag, **(b)** Au, and **(c)** Cu. Each bar corresponds to one of the twenty-two ligands.

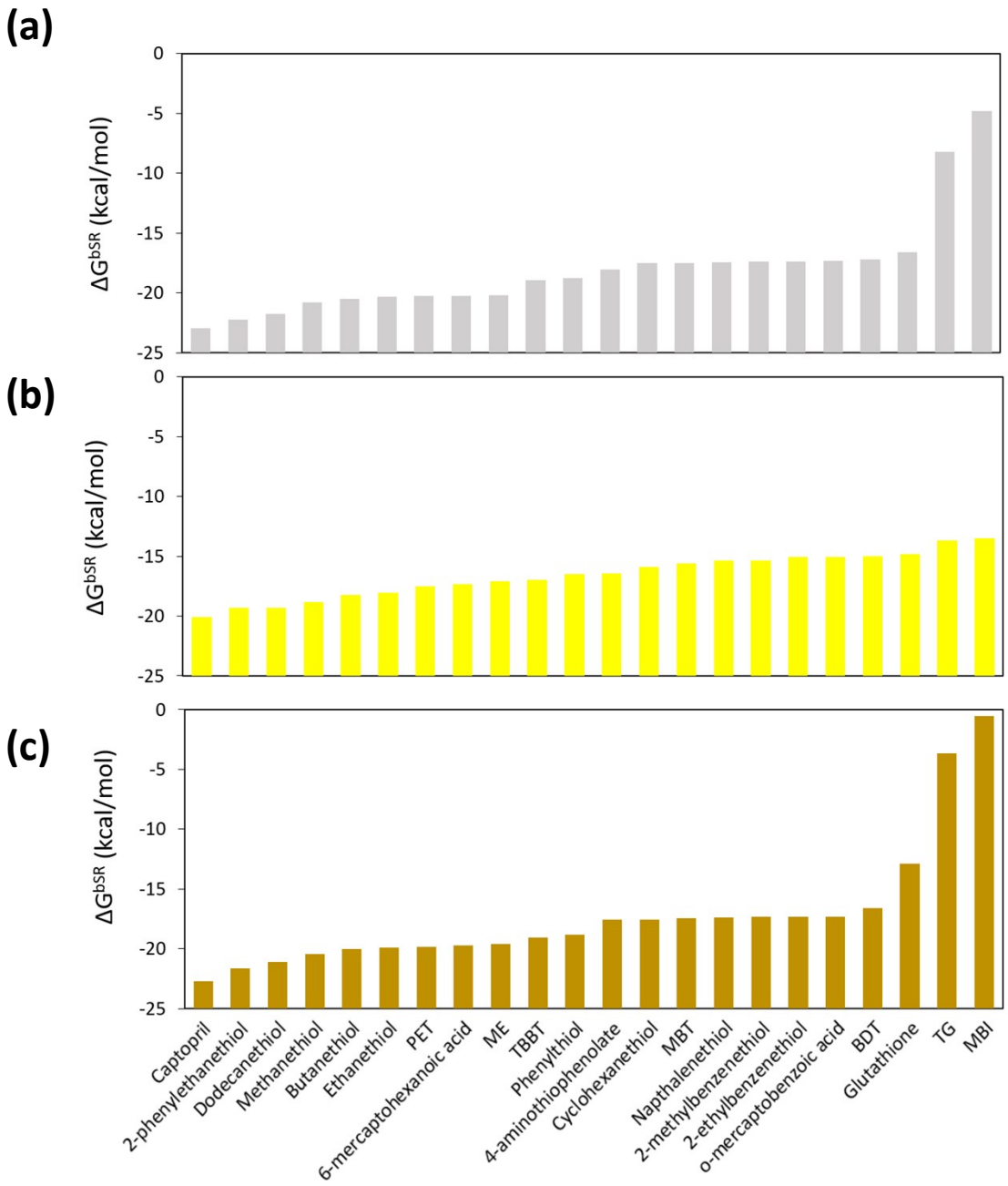

Figure S2. Bar graphs of Gibbs Free Energy of break S-R reaction for **(a)** Ag, **(b)** Au, and **(c)** Cu. Each bar corresponds to one of the twenty-two ligands.

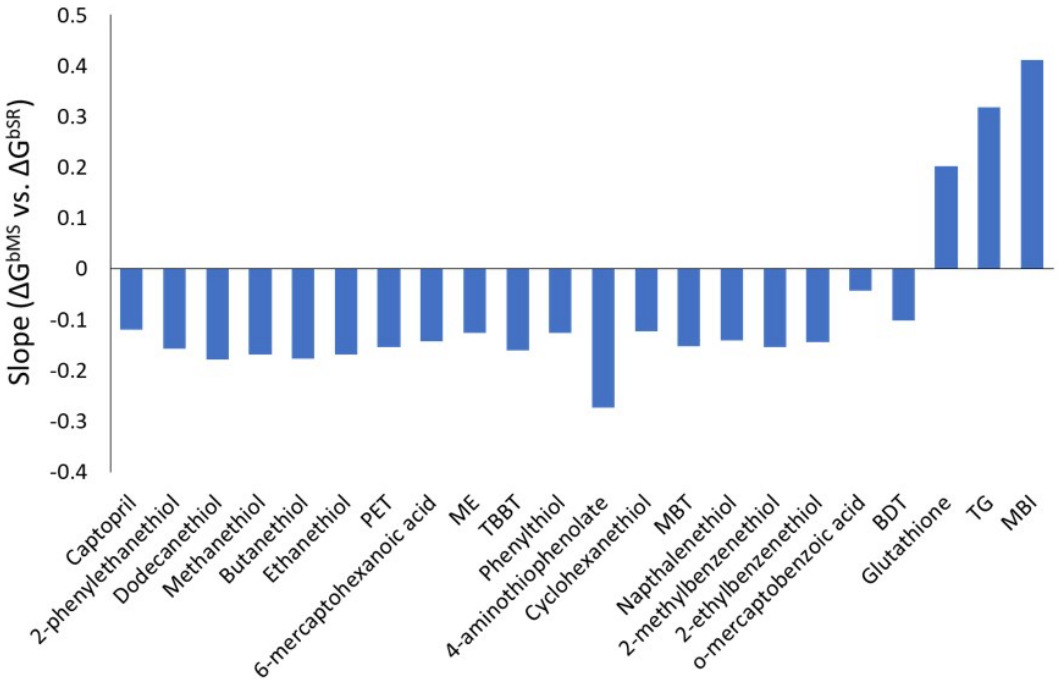

Figure S3. Slope (m) of linear regression line determined from solving $\Delta G^{bMS} = m\Delta G^{bSR} + b$ between metal thiolate complexes with the same ligand (Au-SR, Ag-SR, Cu-SR). Each bar represents one of the twenty-two ligands studied.

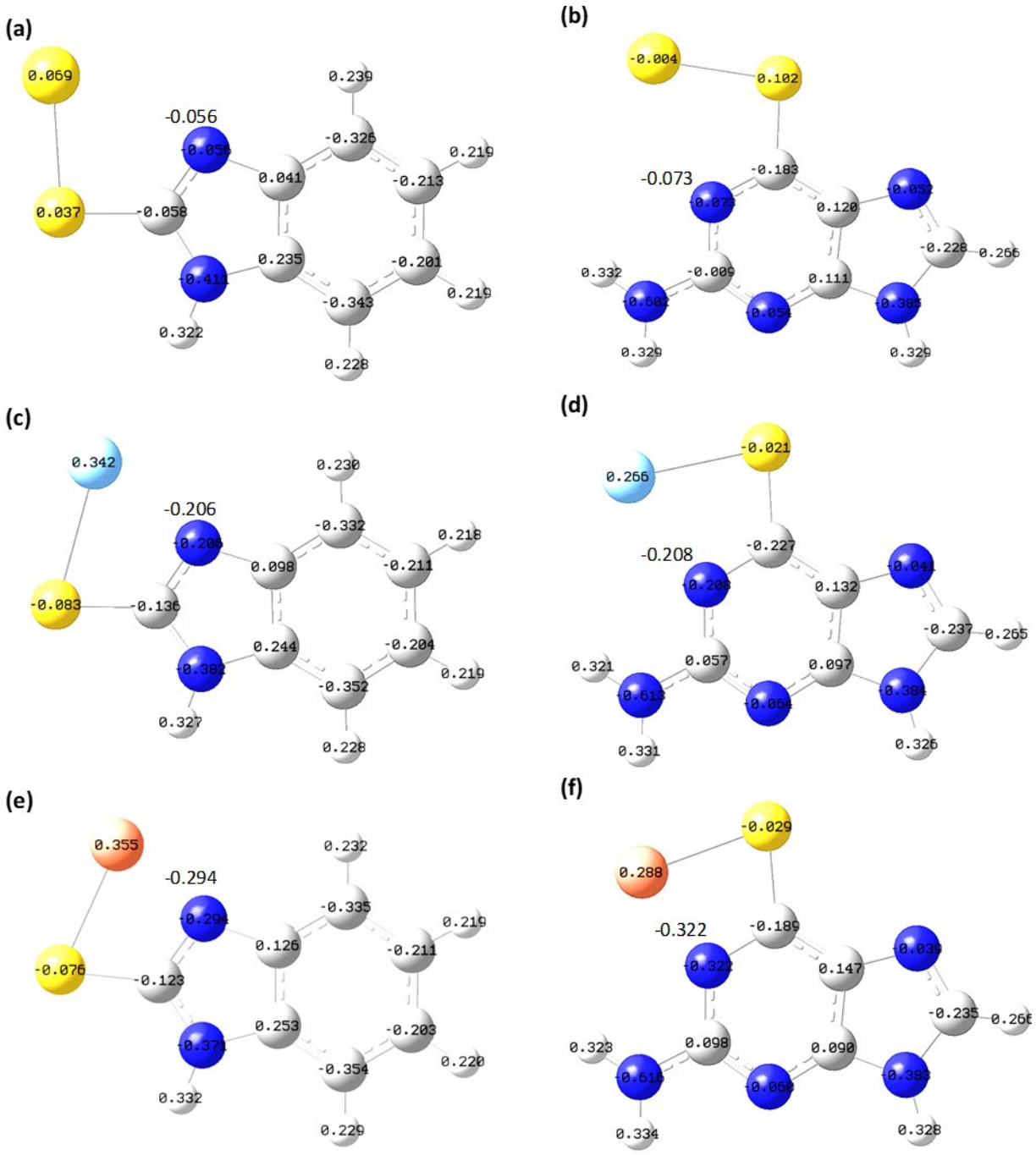

Figure S4. Mulliken Charge distribution on metal thiolate complexes for: **(a)** AuMBI, **(b)** AuTG, **(c)** AgMBI, **(d)** AgTG, **(e)** CuMBI, **(f)** CuTG.

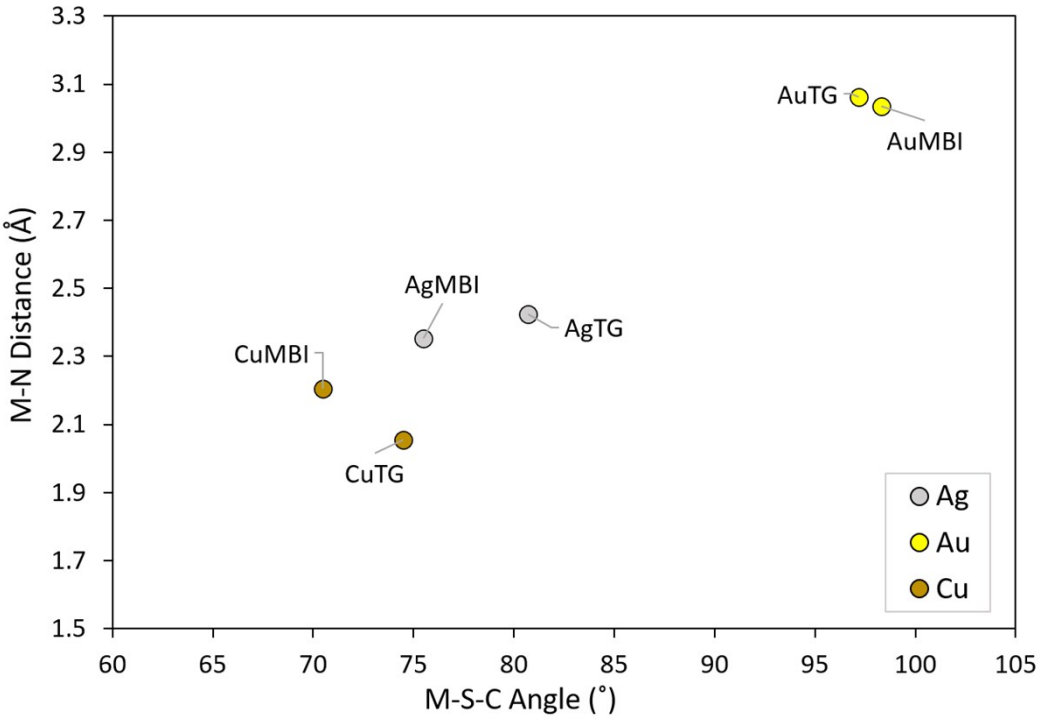

Figure S5. Metal-Sulfur-Carbon (M-S-C) bond angle versus Metal-Nitrogen (M-N) distance for metal thiolate complexes for M = Ag, Au, Cu and SR = MBI, TG.

Table S1. Bond order calculations for M-N atoms (M = Au, Ag, Cu; closest N in ligand) for the TG- and MBI-based complexes shown in Figure S4.

Complex	Bond Order
AuMBI	0.063
AuTG	0.056
AgMBI	0.182
AgTG	0.167
CuMBI	0.228
CuTG	0.227

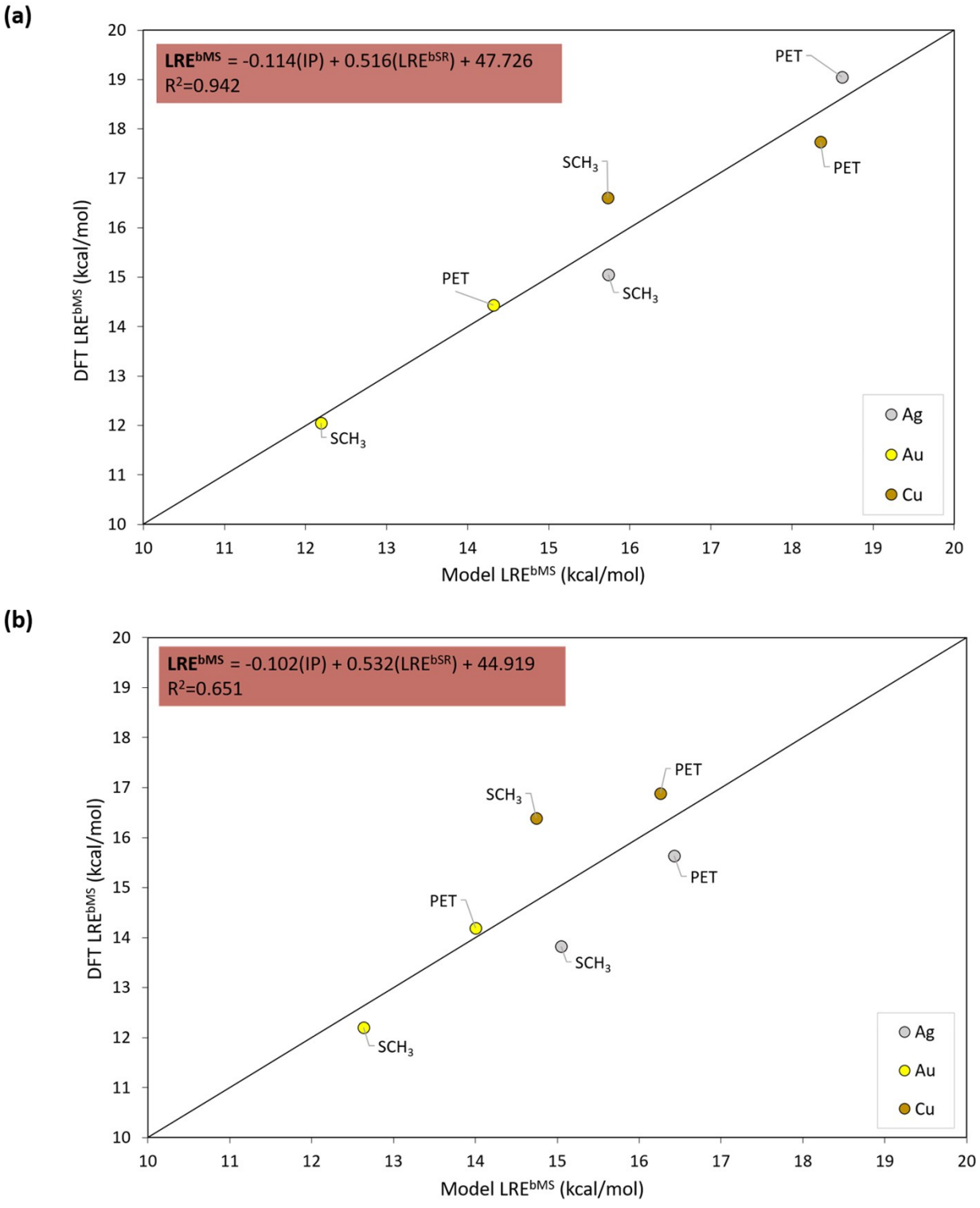

Figure S6. Linear regression models (x-axis Model LRE^{bMS} and equations in red boxes) connecting LRE^{bMS}, LRE^{bSR}, and metal IP for the **(a)** A and **(b)** B ligand removal sites on $[M_{25}(SR)_{18}]^-$. The points are colored according to the three metal types (Ag, Au, Cu) and the ligand types are labeled (SCH_3 and PET).

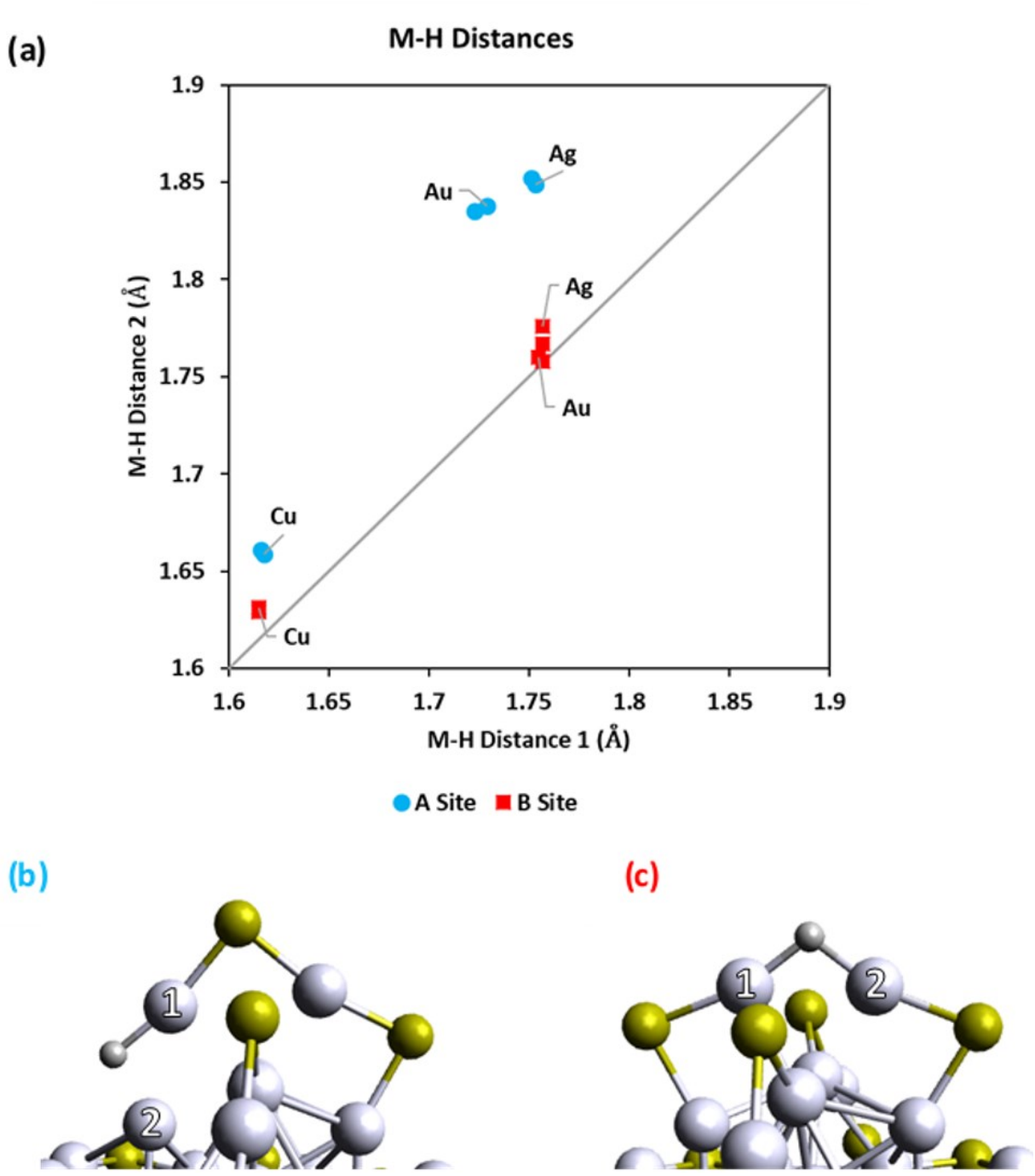

Figure S7. (a) Comparing metal-hydrogen (M-H) distances in products of TPNC break M-S reactions. Gray line corresponds to equivalent distances (parity). The plot shows the difference in configurations between **(b)** A site removal (light blue, 1 = shell and 2 = core metal) and **(c)** B site removal (red, 1 = shell and 2 = shell metal). Ag TPNCs are used to represent the different configurations. R groups are omitted for clarity.

(a)

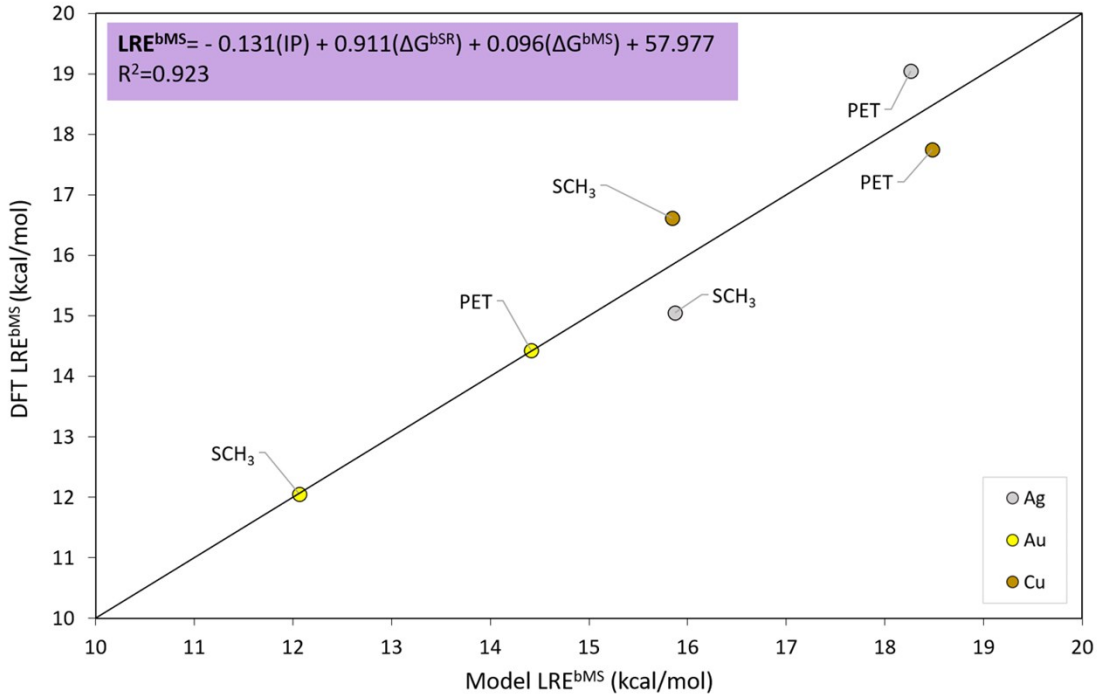

(b)

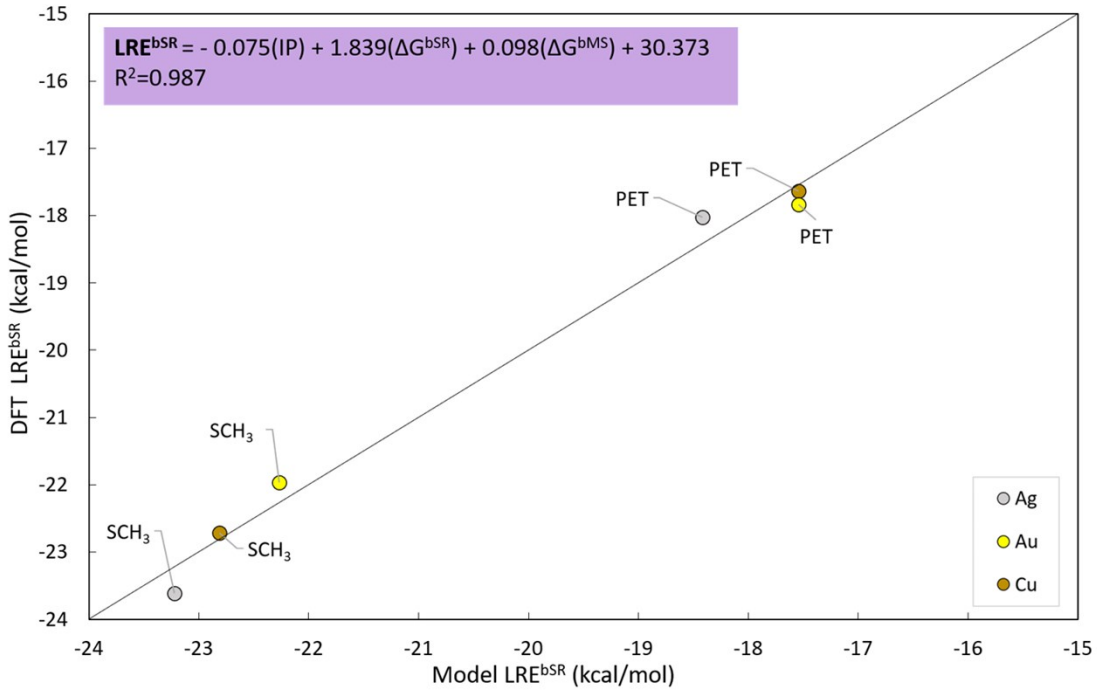

Figure S8. Parity plots of linear regression models (x-axis Model LRE^{bSR}, equations in purple boxes) that reveal strong correlations between ΔG^{bSR}, ΔG^{bMS}, and metal IP with A removal site LREs for the **(a)** break M-S and **(b)** break S-R TPNC reactions.

Investigating Break M-S and Break S-R Kinetics on $MSCH_3$ (M = Au, Ag, Cu)

Methods

The geometries of all intermediates and transition states for the mechanism of the break S-R and M-S bonds for $MSCH_3$ complexes (M = Ag, Au, Cu) were optimized using the B3LYP functional[1, 2] and the LANL2DZ basis set[3]. Frequency calculations were performed to confirm that each stationary point is either a minimum or a transition structure. Intrinsic reaction coordinates (IRC) calculations were used to confirm the path connection between the reactant, product, and transition state[4]. Each structure reported in the reaction coordinate diagrams is the lowest energy conformer as indicated by the calculations. Turnover frequencies (TOF) of the thiolate-protected nanoclusters, were calculated using the energy span model[5] as a means to evaluate the kinetic preference of each mechanism (at room temperature). Images of the 3D molecular structures, on the energy profiles, were generated using CYLView[6].

In order to investigate the mechanisms of hydrogenation reactions, we calculated the transition states (TS) for the SCH_3-based complexes (methanethiol in Figure 1a; Au, Ag, and Cu). Both concerted and stepwise mechanisms were taken into consideration as shown in Figures S9-S11. Our results reveal that the break M-S reaction follows the same concerted mechanism for the three metals – H_2 dissociates onto M and S (TS1, TS5, and TS8 in Figures S9-S11, respectively) followed by the desorption of $HSCH_3$ from the metal. $AuSCH_3$ was found to have the largest barrier (44.5 kcal / mol) compared to $AgSCH_3$ and $CuSCH_3$ (34.1 and 36.3 kcal / mol, respectively), demonstrating the strength of the Au-S bond. A concerted mechanism was also found for break S-R reactions, where H_2 dissociates onto S and C. However, the energy barrier for this mechanism (red line in Figures S9-S11) was found to be very large for the three complexes (> 75 kcal / mol). Instead, stepwise mechanisms were found to be more kinetically favorable for break S-R on the $MSCH_3$ complexes. Of note, the results show that $AuSCH_3$ follows a different stepwise mechanism relative to $AgSCH_3$ and $CuSCH_3$. After dissociating H_2 onto M and S (TS1, TS5, and TS8 in Figures S9-S11, respectively), each hydrogen atom must spillover to an adjacent atom to form the break S-R products (CH_4 + MSH). For the Au complex (Figure S9), the hydrogen transfer occurs in a stepwise manner, involving a hydrogen migration from S to C through TS2 (Figure S9) followed by a second hydrogen migration from Au to S through TS3 (Figure S9). Both transition states have lower energy barriers than the initial H_2 dissociation step (as shown in Figure S9). Conversely, Ag and Cu complexes exhibit a single TS, which is larger than each respective H_2 dissociation step (TS5 and TS8), where both hydrogens are transferred across atoms simultaneously (TS6 and TS9 in Figures S10 and S11, respectively). The metal-dependent mechanisms lead to a difference in reaction preference between complexes. Computing TOFs with the energy span model[5] (given in Figures S1-S3), we find that $AuSCH_3$ prefers the break S-R reaction (Equation 1) while $AgSCH_3$ and $CuSCH_3$ prefer the break M-S reaction (Equation 2). Overall, the reaction coordinate diagrams provide detailed mechanistic understanding of the ligand dissociation reactions in the metal-thiolate complexes.

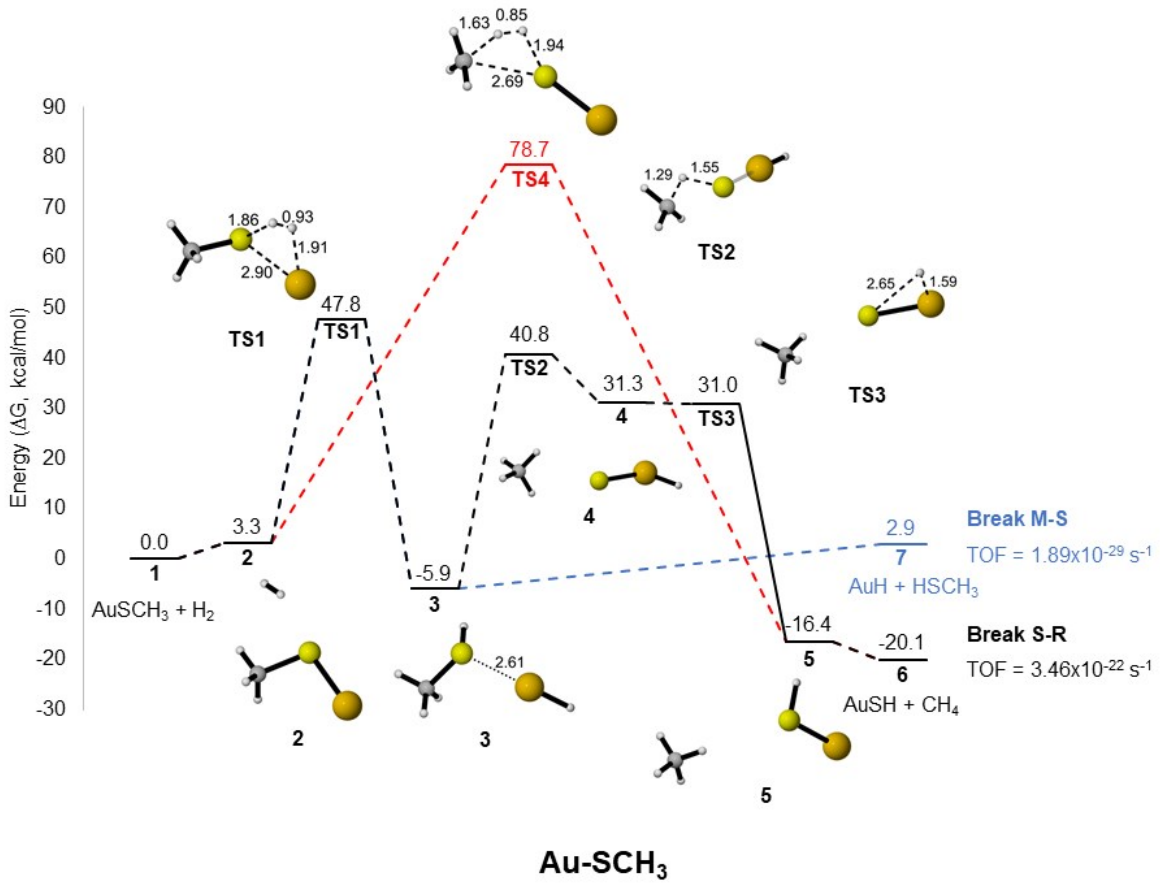

Figure S9. Reaction coordinate diagram depicting break M-S (concerted, blue) and two break S-R (concerted in red and stepwise in black) mechanisms on the $AuSCH_3$ complex.

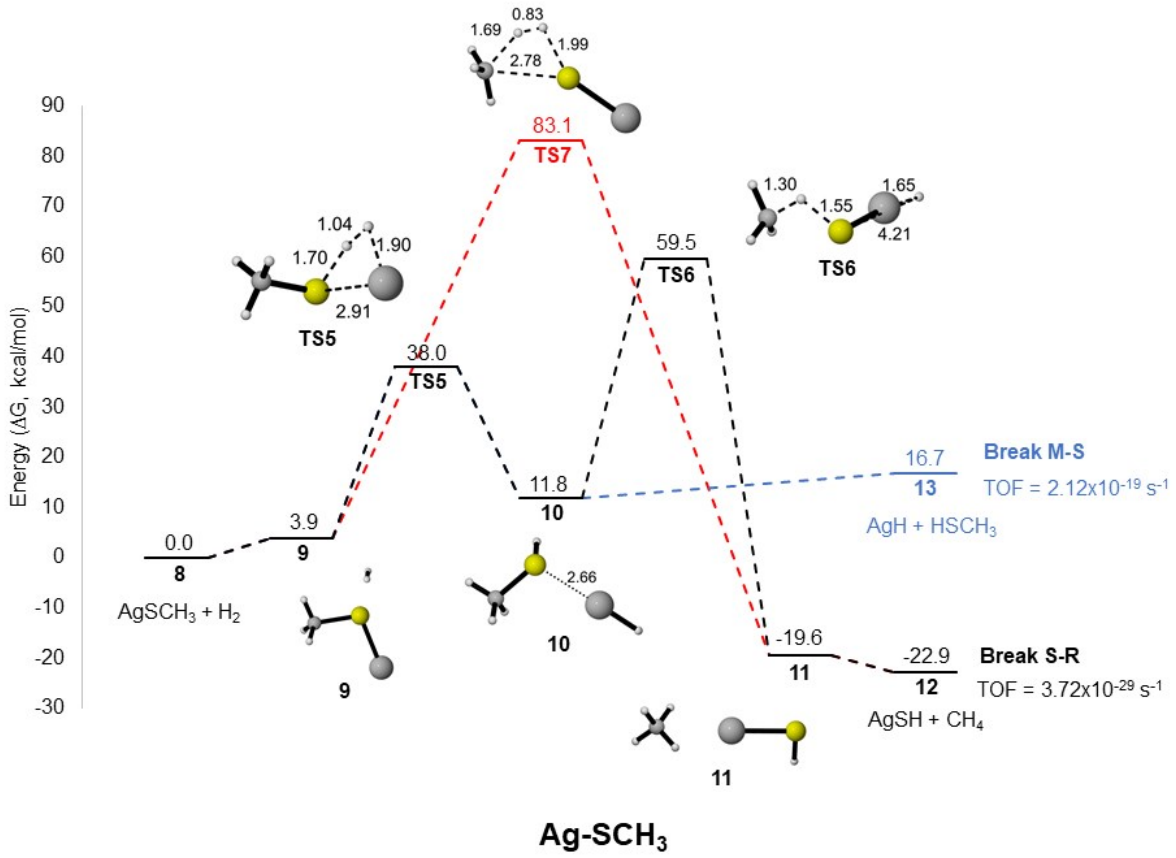

Figure S10. Reaction coordinate diagram depicting break M-S (concerted, blue) and two break S-R (concerted in red and stepwise in black) mechanisms on the $AgSCH_3$ complex.

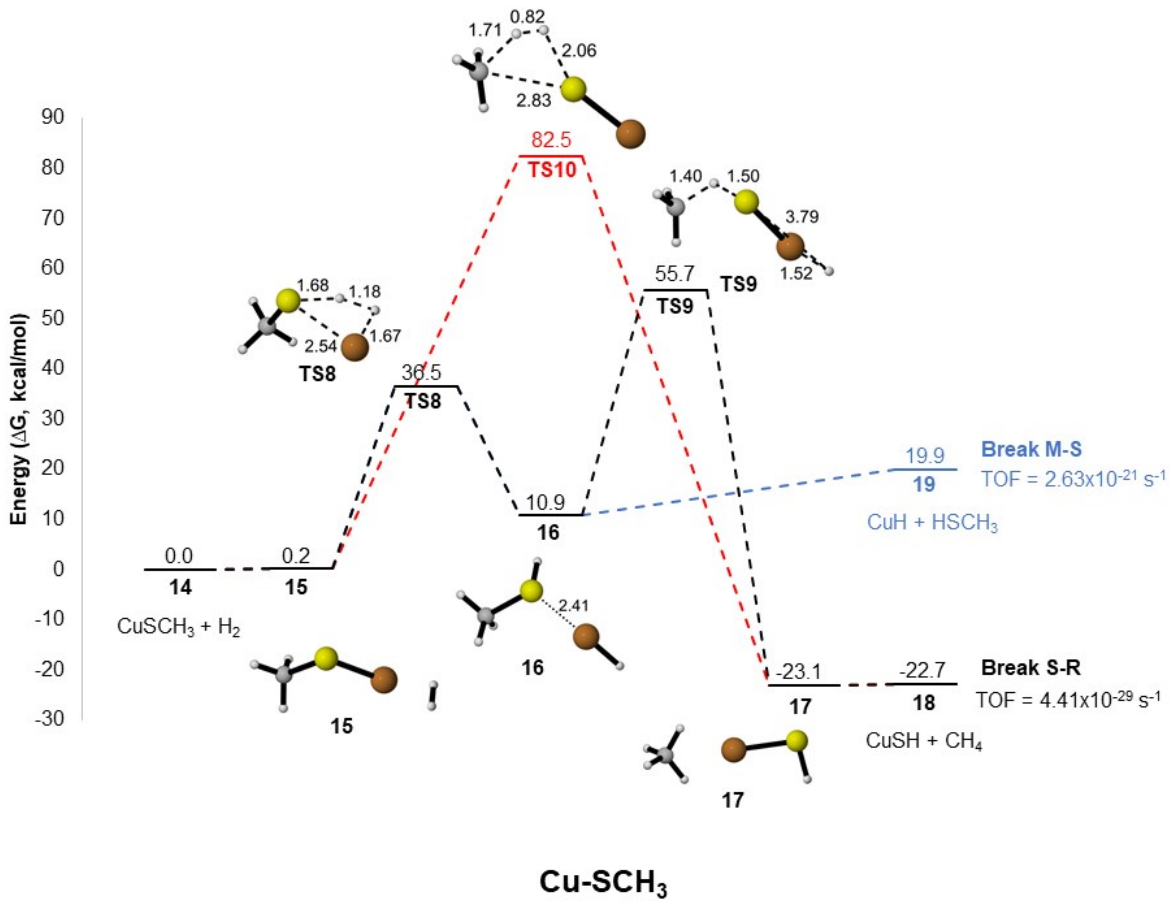

Figure S11. Reaction coordinate diagram depicting break M-S (concerted, blue) and two break S-R (concerted in red and stepwise in black) mechanisms on the $CuSCH_3$ complex.

1. P. J. Stephens, F. J. Devlin, C. F. Chabalowski and M. J. Frisch, *The Journal of Physical Chemistry*, 1994, **98**, 11623-11627.
2. A. D. Becke, *The Journal of chemical physics*, 1993, **98**, 5648-5652.
3. L. E. Roy, P. J. Hay and R. L. Martin, *J Chem Theory Comput*, 2008, **4**, 1029-1031.
4. H. P. Hratchian and H. B. Schlegel, *J. Chem. Phys.*, 2004, **120**, 9918-9924.
5. S. Kozuch and S. Shaik, *Acc. Chem. Res.*, 2011, **44**, 101-110.
6. C. Y. Legault, *Université de Sherbrooke*, 2009, **CYLview 1.0b**, (http://www.cylview.org).